

Effects of turbulent boundary layer thickness on flow around a low-rise rectangular prism

Kyung Chun Kim[†], Ho Seong Ji and Seung Hak Seong

School of Mechanical Engineering, Pusan National University, Pusan 609-735, Korea

(Received January 18, 2005, Accepted August 25, 2005)

Abstract. The effects of upstream velocity profiles on the flow around a low-rise rectangular prism submerged in a turbulent boundary layer have been investigated. Three different boundary layer profiles are generated, which are characterized by boundary layer height, displacement thickness, and momentum thickness. Flow characteristics variations caused by the different layers such as those in turbulent kinetic energy distribution and locations of re-circulating cavities and reattachment points have been precisely measured by using a PIV (Particle Image Velocimetry) technique. Observations were made in a boundary layer wind tunnel at $Re_H=7900$, based on a model height of 40 mm and a free stream velocity of 3 m/s with 15–20% turbulence intensity.

Keywords: turbulent boundary layer; Atmospheric boundary layer (ABL); PIV; flow around a rectangular prism.

1. Introduction

Flows around structures in a turbulent boundary layer are strongly dependent upon approaching flow characteristics as well as the geometric shape of the structures, and this issue has long been an important topic in industrial aerodynamics studies (Bearman and Obasaju 1982, Saathoff and Melbourne 1997, Hosker 1984, Tieleman and Akins 1996, Wu, *et al.* 2001). Knowledge about basic flow structures, such as recirculating cavities, and information on turbulence characteristics around a structure in an atmospheric boundary layer are of practical importance to many wind engineering problems. Dynamic wind loadings and their responses and the prediction of pollutant dispersions are typical examples of such problems. For this study, the success of physical modeling of a turbulent atmospheric boundary layer should be preceded.

Upstream wind effects on the dynamic loadings and responses were clearly observed to be significant in a study on high-rise building (Whitebread and Scruton 1965). In the study, the uniform flow and the boundary layer flow were comparable. The shape of an upstream velocity profile would affect the flow structure around the building and the resultant wind loadings and consequently induce significantly different dynamic behaviors in the structure. A boundary layer flow induces galloping while a uniform flow does not. When a building is higher than a boundary layer thickness (height), it is important to precisely scale the velocity profile and the boundary layer

[†] Professor, Corresponding Author, E-mail: kckim@pusan.ac.kr

height relative to the building height in a wind tunnel model study.

In low-rise buildings, however, no such dynamic behavior of swaying motion, for instance, galloping occurs. Instead, localized dynamic surface loading dominates the overall structural behavior. The localized loadings are directly affected by the flow structures around and near a building envelop such as separation bubbles and reattachment locations. Again, the flow structures will be affected by the approaching wind profiles. In such a case, however, particularly if they are completely submerged in the boundary layer, the effect of the boundary layer height may not be significant contrary to the case of high-rise structures. In fact, it is hard for the building to sense the change of the boundary layer height that is rather sensitive to the definition of the layer, for example, $0.99U$ or $0.991U$. In this case, the most important property to affect the flows and localized dynamic loadings is the characteristics of turbulence and the mean velocity profile of the approaching flow near the building height. Turbulence is a major characteristic of an atmospheric surface layer, which makes it not only difficult to do physical modeling of scaled flows but also difficult to do flow measurements. It is necessary to properly scale an upstream velocity profile that is characterized by momentum thickness or displacement thickness relative to the model height as well as turbulence characteristics such as turbulence intensity, integral scales, etc.

One typical example of a such low-rise rectangular prism is the Texas Tech University (TTU) experimental building. The building is located completely under the turbulent atmospheric surface layer. Comprehensive research on the TTU building has been reported, which include full-scale measurements, wind tunnel modeling of ABL and flows and loadings on the building, and computational studies and their comparisons (Whitebread and Scruton 1965, Cermak and Cochran 1992, Tieleman, *et al.* 1996, Levitan and Mehta 1992, Bienkiewicz 1992). It is generally agreed that the mean pressure distribution on the envelope can be fairly accurately obtained using a scaled model under a properly modeled atmospheric boundary layer in a wind tunnel. Such was reasonably verified by measuring surface pressures in full scale and model scales. Also, some basic flow structures above a roof surface such as the reattachments of conical roof vortices were conjectured by performing flow visualizations such as oil painting in a wind tunnel. A study on interactions between conical vortices and induced surface pressures was attempted by using smoke visualization and simultaneous measurements of surface pressure (Banks, *et al.* 2000). In those studies, a common difficulty may be measuring turbulence close to the surface and in the wake zone. Furthermore, it is difficult to measure appreciable changes in the turbulent flow field by the different upstream flow characteristics.

This study used a PIV technique to measure the flow field and to precisely estimate the effects of the approaching flow on the basic flow structure and turbulence kinetic energy distribution around a rectangular prismatic model.

2. Experimental setup

2.1. Boundary layer generation

The experiments were conducted in a atmospheric boundary layer wind tunnel at Pusan National University, Korea. The tunnel features a $2.1 \times 2.1 \times 20$ m test section with an adjustable ceiling and a maximum velocity of 23 m/s. For the generation of a boundary layer, four vortex generators (950 mm height, 80 mm width) and a fetch of roughness chain (15 mm height, 300 mm spacing) were used as shown in Fig. 1.

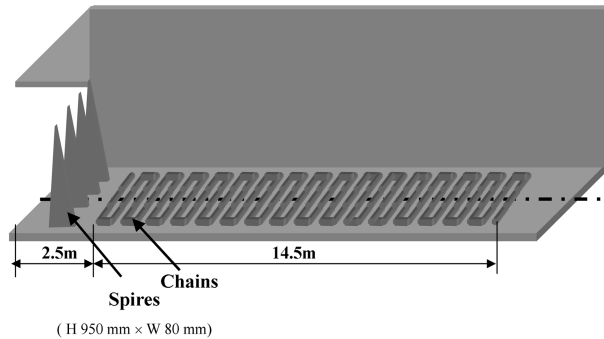


Fig. 1 Schematic of a boundary layer generation system

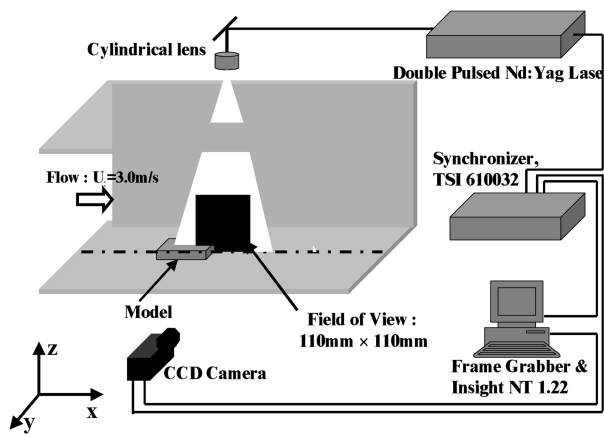


Fig. 2 Schematic of an experimental set-up

A sketch of the experimental arrangement showing the locations of a model, a camera, and a measurement plane is given in Fig. 2. A prismatic model 40 mm in height, 95 mm in width, and 140 mm in length is located 18 m downstream from the entrance. The model was made of glass in order to minimize the reflection of laser beams. A CCD camera was placed perpendicular to the laser sheet plane, as shown in Fig. 2. The vertical sheet aligned with the flow direction was illuminated by a laser beam passing through a cylindrical lens located above the test section.

For tracer particles, droplets of olive oil were used. The olive oil, because it is non-toxic, non-corrosive, non-abrasive, chemically non-volatile, satisfies the general specifications of PIV seeding particles. Also, olive droplets with a diameter of about 1–2 μm give an adequate aerodynamic response to velocity gradients in the flow as seen in the wind tunnel study. To generate the tracer particles, two Laskin nozzle chambers were made. Each chamber had 6 nozzles. An air distributor was introduced at the entrance of the chamber for a uniform distribution of compressed air to the six nozzles.

2.2. PIV measurement setup

The PIV system used in this study consisted of a double-pulsed Nd-Yag laser with a maximum power of 200 mJ per pulse, a PIVCAM 10-15 CCD camera, a Synchronizer TSI 610032, and a

personal computer. The camera captures an image with a pixel resolution of $1k \times 1k$. PIV measurements were made in two different areas with slightly different settings: a thick boundary layer and the thin and medium thickness boundary layer.

For the thin and medium thickness boundary layer, the time interval between two successive images was $150 \mu\text{s}$. A 80–200 mm Nikon telephotographic lens was used to capture a $110 \text{ mm} \times 110 \text{ mm}$ field of view. In one plane, 1,020 image frames (510 velocity fields) were captured and processed. The interrogation window size for velocity calculation was set to 24×24 pixels, and 50% of overlap was permitted. A total of 7,056 velocity vectors were interrogated and the spatial resolution of the velocity data was 1.3 mm.

For the thick boundary layer, the time interval between two successive images was $200 \mu\text{s}$. A 80–200 mm Nikon telephotographic lens was used to capture a $280 \text{ mm} \times 280 \text{ mm}$ field of view. In one plane, 2,040 image frames (1,020 velocity fields) were captured and processed. The interrogation window size for velocity calculation was set to 24×24 pixels, and 50% of overlap was permitted. A total of 3,969 velocity vectors were interrogated, and the spatial resolution of the velocity data was 1.3 mm.

After removing spurious vectors, ensemble averaging and other statistical calculations were conducted by using post-processing program PIV-ACE V1.0, which was developed at the laboratory and based on the two-frame cross-correlation method. The PIV parameters for the three boundary layers are summarized in Table 1.

3. Results and discussion

3.1. Approaching flows

Three different approaching flows were generated by the roughness on the floor and the spires at the entrance of the 18 m-long test section. A wire mesh screen was added at the entrance of the test

Table 1 Boundary layer characteristics and PIV parameters

Case	Thick	Medium	Thin
U_∞	3 m/s	3 m/s	3 m/s
Time interval	200 μs	150 μs	150 μs
# of ensemble	1020	510	510
Field of view	$280 \text{ mm} \times 280 \text{ mm}$	$110 \text{ mm} \times 110 \text{ mm}$	$110 \text{ mm} \times 110 \text{ mm}$
mm/pixel	0.27	0.11	0.11
# of vector	3,969	7,056	7,056
Interrogation window	24×24	24×24	24×24
δ	650 mm	270 mm	36.5 mm
δ^*	117.4 mm	41.3 mm	7.6 mm
Θ	78 mm	30 mm	2.46 mm
Shape factor	1.50	1.37	3.09
Re_δ	1.1×10^5	4.32×10^4	6.7×10^3
u^*	0.085 m/s	0.092 m/s	0.14 m/s
$\tau_w [\text{N/m}^2]$	8.67×10^{-3}	1.02×10^{-2}	2.4×10^{-2}
Re_H	7.9×10^3	7.9×10^3	7.9×10^3

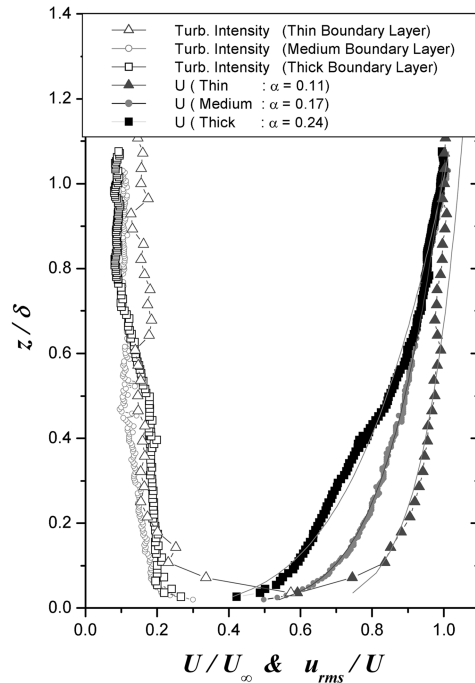


Fig. 3 Approaching boundary layer

section, which effectively helped to form a curved boundary layer profile near the floor. Fig. 3 compares the vertical distributions of streamwise velocities of the three approaching flows that were scaled by boundary layer thickness. The variations in the profile shape were well distinguished by different power law exponents: 0.11, 0.17, and 0.24. The turbulence intensity was about 20% at the model height (40 mm) and tended to remain at 20% throughout the building height.

The thick boundary layer ($\delta=650$ mm) was obtained by the floor roughness and the spires as depicted in Section 2.1 and the screen at the entrance. The Reynolds number based on the boundary layer thickness was 1.1×10^5 . The displacement thickness (δ^*) and the momentum thickness (θ) are 117.4 mm and 78 mm, respectively.

The medium thickness boundary layer ($\delta=270$ mm) was obtained by no floor roughness elements and no spires and only by the floor surface roughness and the screen at the entrance. The Reynolds number based on the boundary layer thickness was 4.32×10^4 . The displacement thickness (δ^*) and the momentum thickness (θ) are 41.3 mm and 30 mm, respectively.

The thin boundary layer ($\delta=36$ mm) was obtained in a somewhat tricky method, while the thickest and the medium thickness layers were obtained by natural growth through the long upstream fetch. The layer was obtained at a flat plate located at the 70 cm height above the floor and at the end of the fetch where the turbulent boundary layer developed. Thus a very thin boundary layer with similar turbulence intensity was obtained. The Reynolds number based on the boundary layer thickness was 6.7×10^3 . The displacement thickness (δ^*) and the momentum thickness (θ) are 7.6 mm and 2.46 mm, respectively.

The different shape of the turbulent boundary layer was characterized by the shape factors ($\delta^*/\theta=1.5, 1.4, 3.1$) and the power law exponents ($\alpha=0.24, 0.17, 0.11$). The power law exponents

correspond roughly to suburban terrain, open terrain, and coastal areas, respectively, in wind engineering applications.

It should be noted that the three different boundary layer profiles were obtained by scaling the vertical distributions of the mean velocity by different boundary layer heights. Thus, the profile shapes do not represent the actual variability of the upstream velocity approaching the 4 cm-height model. The model will sense much more different velocity gradients near the model height. The thinnest layer would be close to the almost uniform flow, as evidenced by the displacement thickness of 7.6 mm. In Fig. 3, the high turbulent intensity at two measurement locations near the surface is due to the effect of leading edge of the plate. Also the distinguished difference in plot near the wall is partially due to the use of different length scale of δ in the different layer. However the effect of such erroneous high intensity would be limited to 3 mm layer (7% of the model height) and not significant in the overall flow character. The three different boundary layers are summarized in Table 1.

3.2. Mean flow structures

Mean velocity fields were obtained for the three different approaching flows, which are referred to in this paper as the thick boundary layer flow, medium thickness boundary layer flow, and thin boundary layer flow. All these flow fields were obtained at the symmetric plane passing the centerline of the model in the direction as shown in Fig. 2.

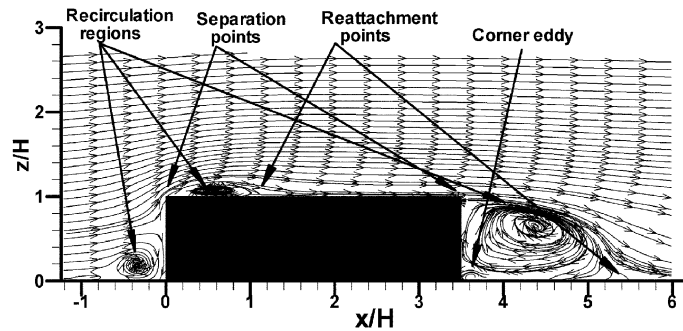


Fig. 4 Streamlines around the model (thick boundary layer flow)

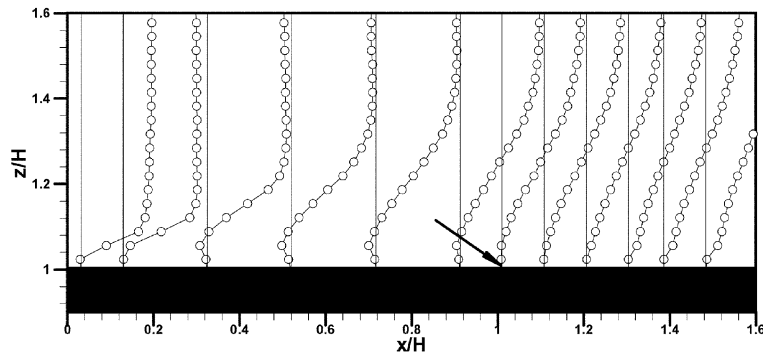


Fig. 5 Velocity distribution of the flow over the roof (thick boundary layer flow)

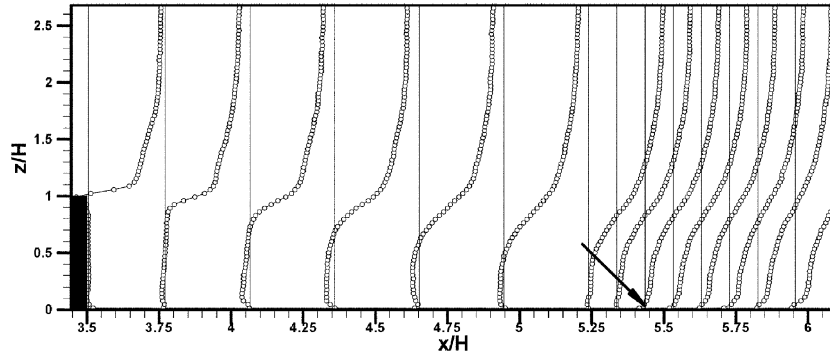


Fig. 6 Velocity distribution in the wake region (thick boundary layer flow)

Figs. 4, 5, 6 show the flow fields for the thick boundary layer. In Fig. 4, streamlines around the model reveal a clear view of mean flow structures, including three recirculation regions. Fig. 5 shows a vertical distribution of streamwise mean velocity in the roof recirculation region. The location of reattachment was found by investigating $du/dy=0$ along the roof surface and is indicated

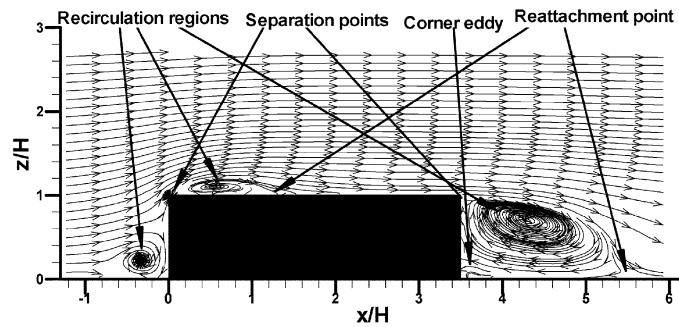


Fig. 7 Streamlines around the model (medium thickness layer flow)

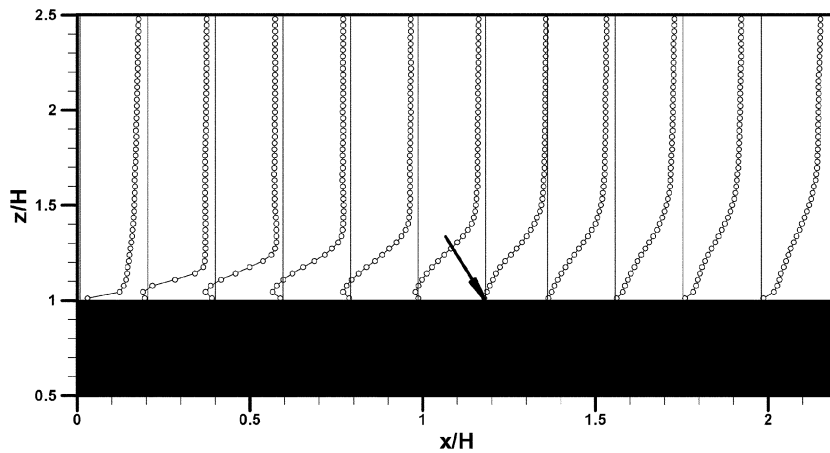


Fig. 8 Velocity distribution of the flow over the roof (medium thickness layer flow)

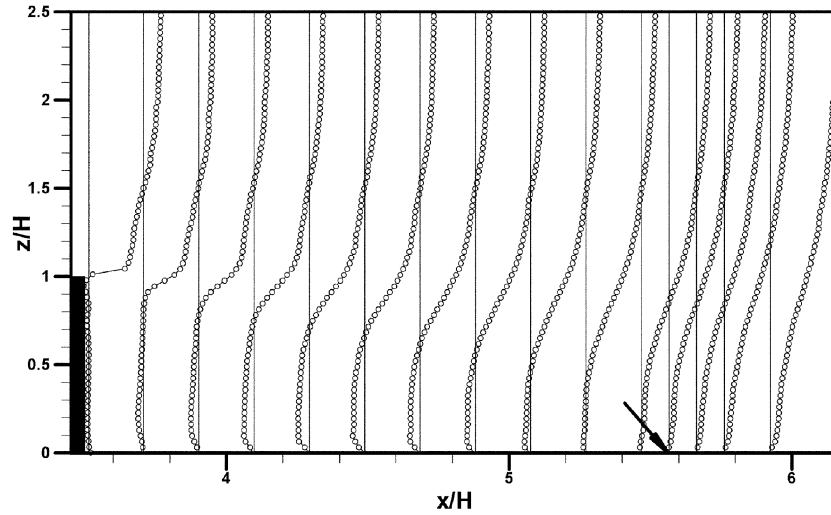


Fig. 9 Velocity distribution in the wake region (medium thickness layer flow)

in the figure by a solid arrow. The reattachment on the roof occurs at around $1.01H$. Fig. 6 represents the recirculation region behind a building and the reattachment location. The reattachment on the floor in the downstream occurs at around $5.43H$, which corresponds to $1.93H$ from the leeward face of the model.

Figs. 7, 8, 9 correspond to the medium thickness boundary layer flow, and Figs. 10, 11, 12 to the thin boundary layer flow. In all three cases, overall flow structures are similar, even for the significantly different approaching flows. However, appreciable changes in some critical locations were observed. As the boundary layer thickness decreases, the size of the roof recirculation region increases. The thickness of the roof recirculation increases ($0.19H \rightarrow 0.21H \rightarrow 0.27H$), and the length of the recirculation also increases ($1.01H \rightarrow 1.18H \rightarrow 1.57H$). The increase in length was about 45%. The decrease of the boundary layer thickness also increases the size of the wake recirculation region in the streamwise direction. The reattachment location on the floor moves downstream ($5.43H \rightarrow 5.56H \rightarrow 5.84H$) as the boundary layer thickness decreases.

When a reattachment point exists on the roof, it is expected that a thinner boundary layer containing a relatively large momentum induces a bigger roof recirculation cavity. The bigger

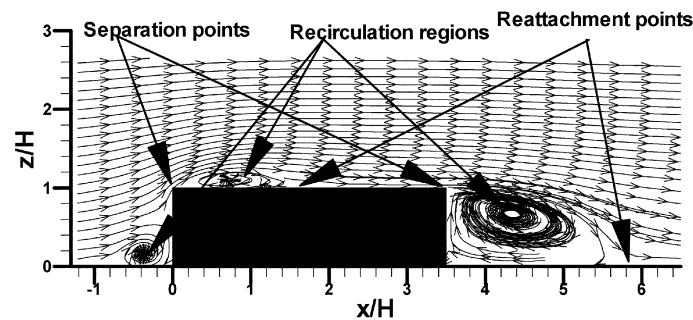


Fig. 10 Streamlines around the model (thin boundary layer flow)

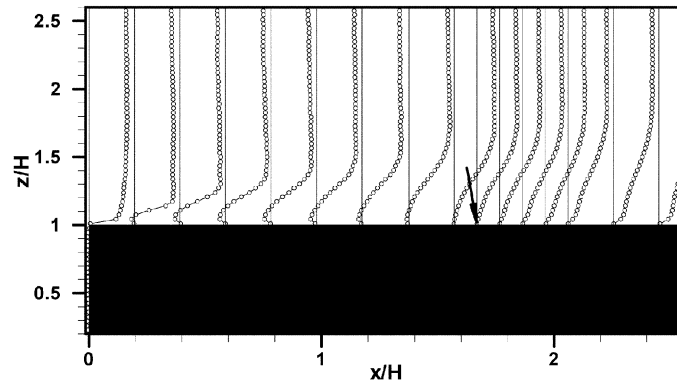


Fig. 11 Velocity distribution of the flow over the roof (thin boundary layer flow)

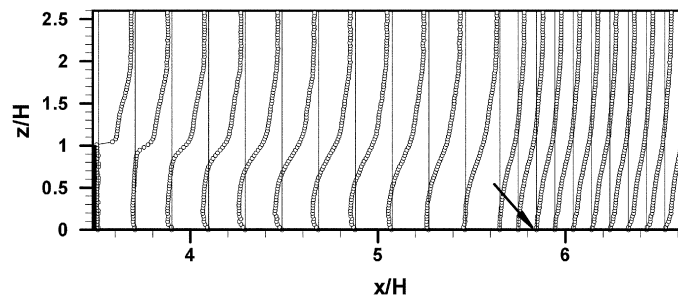


Fig. 12 Velocity distribution in the wake region (thin boundary layer flow)

roof recirculation cavity in turn induces a bigger wake recirculation cavity downstream. An early reattachment on the roof by a small cavity results in the longer distance of surface resistance where the distance is between the reattachment point and the downstream roof edge. Then, the long distance reduces the magnitude of linear momentum at the end of the roof. In the contrast, the late reattachment by a big cavity reduces the loss of linear momentum by the surface resistance and thus enables that to maintain a relatively bigger momentum at the edge. The bigger momentum in the streamwise direction at the roof edge helps to form a bigger cavity in the wake region.

One of the recirculations is a standing vortex in the vicinity of the windward face and the floor. Approaching air is deflected on the windward face of a model building centering around a stagnation point. Part of the air is deflected downward and forms a vortex that extends laterally and is developed into a horseshoe vortex. The stagnation point depend upon the location of the stagnation points moves down ($0.77H \rightarrow 0.67H \rightarrow 0.56H$) as the boundary layer thickness decreases.

Finally, Figs. 13 and 14 reveal detailed flow structures and summarize the precise variation in some critical locations with the boundary layer thickness variation.

3.3. Turbulent kinetic energy distribution

The distribution of turbulent kinetic energy provides dynamic information on turbulent flow fields around a model. *TKE* can be defined calculated by the following approximation.

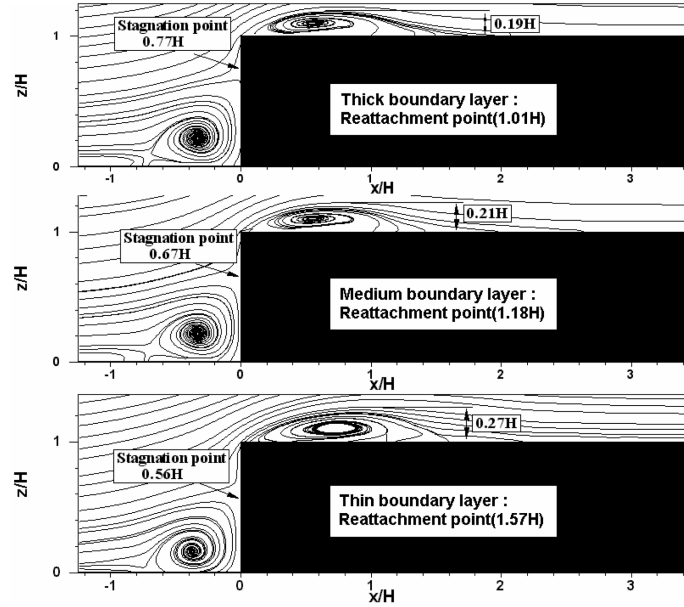


Fig. 13 Comparison of streamlines in the upstream side for the three boundary layer flows

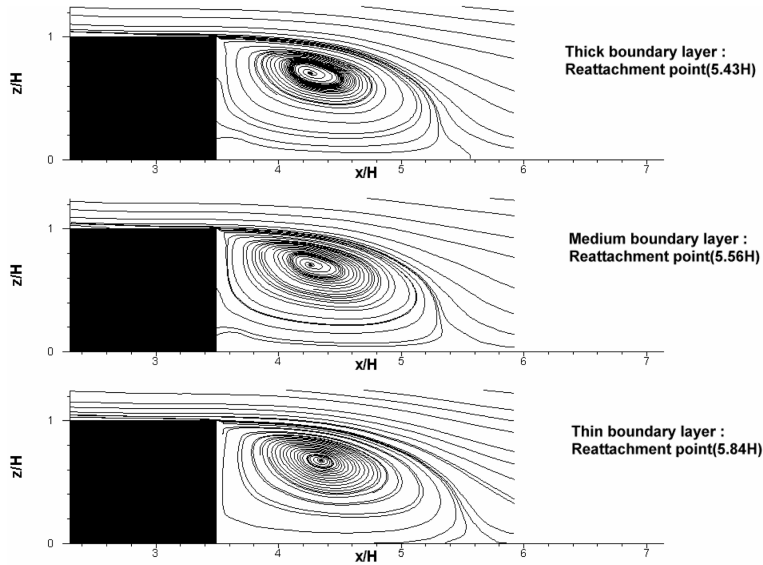


Fig. 14 Comparison of streamlines in the downstream side for the three boundary layer flows

$$\begin{aligned}
 TKE &= \frac{1}{2}(u^2 + v^2 + w^2) \\
 &= \frac{3}{4}(u^2 + w^2),
 \end{aligned}$$

where $v^2 = 1/2(u^2 + w^2)$ are assumed because v cannot be measured on the x - z measurement plane.

This assumption appears reasonable based on the wind tunnel data. In turbulence intensity profiles of a shear layer, Arie and Rouse (1956), three directional components- u , v and w - have similar shapes in distribution. The magnitude of the v component was also found to be somewhere between the u and the w .

Figs. 15-18 represent TKE distributions around a model for the three boundary layer flows. The value is non-dimensionalized by U^2 . The maximum TKE occurs at the roof recirculation region. The level of TKE in the wake region is relatively low. In Fig. 15 for the thick boundary layer flow, the maximum TKE in the roof recirculation region was 0.57, which is about 68% higher than 0.34 found in the corner region near the windward face of the building and higher than 0.23 found in the wake region downstream.

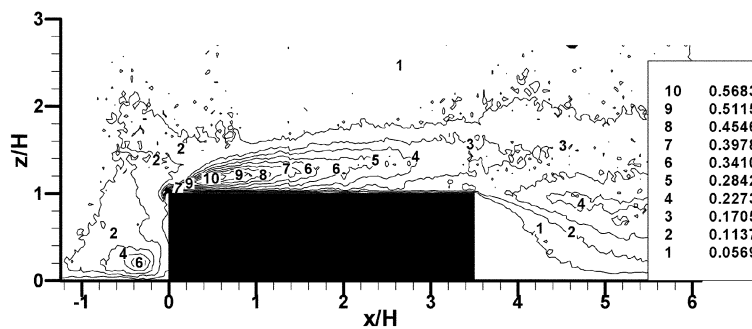


Fig. 15 Distribution of TKE (thick boundary layer flow)

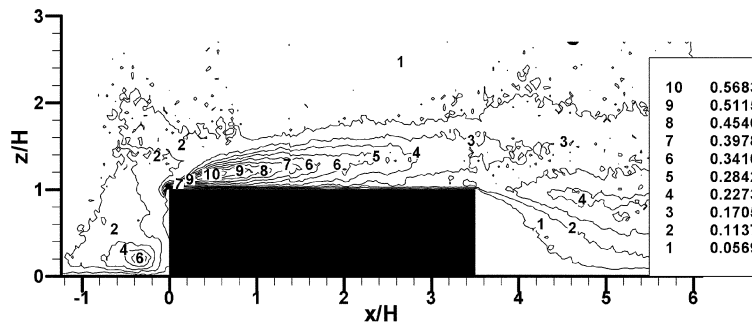


Fig. 16 Distribution of TKE (medium thickness layer flow)

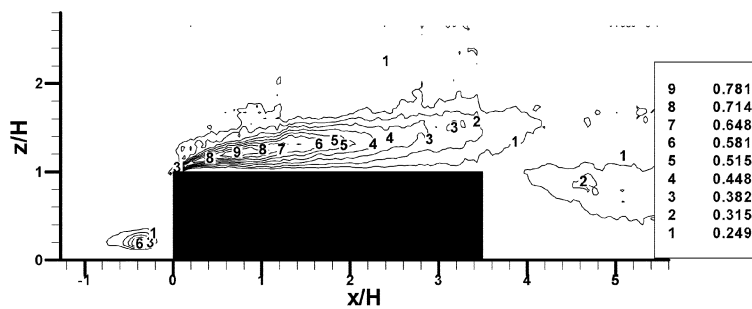


Fig. 17 Distribution of TKE (thin boundary layer flow)

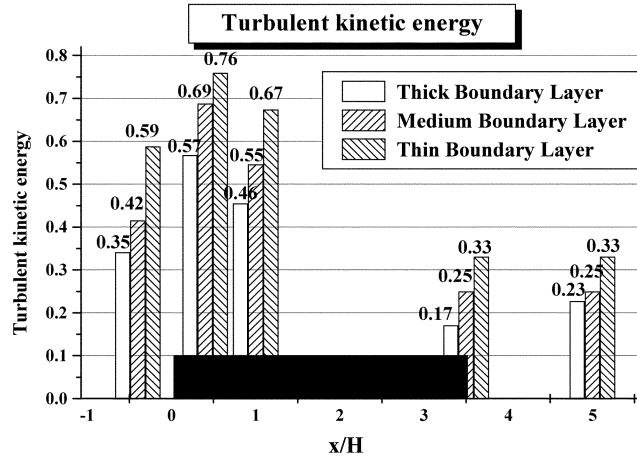


Fig. 18 Comparison of TKE at several critical locations for the three boundary layer flows

The maximum TKE in the roof was found near the upper boundary of the roof recirculation cavity where the flow separated from the sharp roof edge is accelerated and the separated layer has a large velocity gradient. The location of the maximum TKE is consistent with the experimental results for the shear layer separated from a wall with a sharp edge located normal to the flow, Arie and Rouse (1956). The highest TKE generated near the upwind edge appears dispersed and its intensity is spread as the flow moves downstream. The envelop of the substantial influence of the TKE is quite similar to the roof wake boundary reported by Wilson (1979). As the boundary layer thickness decreases, in other words, as the approaching flow momentum increases, the level of TKE over most of the region increases as shown in Figs. 16 and 17, which respectively correspond to the medium thickness and the thin layer flows. The pattern of the relative distribution of the maximum TKE in the three recirculation regions was unchanged. Fig. 18 compares the TKE distribution for the three cases at some critical locations. At the upstream corner, the maximum TKE for the thick boundary layer is 1.2 and 1.7 times higher than those for the medium and thin layers, respectively. At the roof separation, the maximum TKE for the thick boundary layer is 1.2 and 1.3 times higher than those for the medium and thin layers, respectively. At the roof reattachment, the maximum TKE for the thick boundary layer is 1.2 and 1.4 times higher than those for the medium and thin layer respectively. At the roof separation downstream, the maximum TKE for the thick boundary layer is 1.5 and 1.9 times higher than those for the medium and thin layers, respectively. At the wake region, the maximum TKE for the thick boundary layer is 1.1 and 1.5 times higher than those for the medium and thin layers, respectively.

4. Conclusions

To investigate the effects of boundary layer thickness on flow around a prismatic model building, three turbulent boundary layer flows were generated. Resulting three flow fields were compared using the streamline pattern of mean velocity fields and the TKE distribution. For such significantly different mean velocity profiles, quite similar shapes of flow structure were obtained, and the precise variations were measured by the PIV technique. Based on the detailed flow structures in recirculation zones and precise measurements of several critical locations and the TKE , the study

detected changes in the flow structure, depending upon the approaching flow. Two key features, including variation range, are summarized below:

- (1) As the boundary layer thickness decreases, the following were found: the reattachment location on the roof moves downstream ($1.01H \rightarrow 1.18H \rightarrow 1.57H$); the height of the roof recirculation cavity increases ($0.19H \rightarrow 0.21H \rightarrow 0.27H$); the reattachment location on the ground floor moves downward ($5.43H \rightarrow 5.56H \rightarrow 5.84H$); and the stagnation location on the windward face moves downward ($0.77H \rightarrow 0.67H \rightarrow 0.56H$).
- (2) As the boundary layer thickness (momentum thickness) decreases, the average *TKE* level increases all over the flow field. The maximum *TKE* occurs at the roof recirculation region. The second largest *TKE* occurs at the upstream corner vortex region. The third largest occurs at the wake region. A quantitative variation of the *TKE* was obtained as a function of the change boundary layer thickness. For example, the maximum *TKE* for the thin boundary layer flow is 1.3 times higher than that for the thick boundary layer flow.

Acknowledgements

This work was supported by Brain Korea 21.

References

- Bearman, B.E. and Obasaju, E.D. (1982), "An experimental study of pressure fluctuations on fixed and oscillation square-section cylinders", *J. Fluid Mech.*, **119**, 297-321.
- Saathoff, P.J. and Melbourne, W.H. (1997), "Effects of free-stream turbulence on surface pressure fluctuations in a separation bubble", *J. Fluid Mech.*, **337**, 1-24.
- Hosker Jr., R.P. (1984), "Flow and diffusion near obstacles", in Darryl Randerson (Eds.), *Atmospheric Science and Power Production*, DOE/TIC-27601, U.S. Department of Energy, 241-326.
- Tieleman, H.W. and Akins, R. (1996), "The effect of incident turbulence on the surface pressures of surface-mounted prisms", *J. Fluid Struct.*, **10**, 367-393.
- Wu, F., Sarkar, P.P., Mehta, K.C. and Zhao, Z. (2001), "Influence of incident wind turbulence on pressure fluctuations near flat-roof corner", *J. Wind Eng. Ind. Aerodyn.*, **89**, 403-420.
- Whitebread, R.E. and Scruton, C. (1965), "An investigation of the aerodynamics stability of a model of the proposed tower blocks for the world trade center", New York, Aero Report No. 1165, National Physical Laboratory, Teddington, July.
- Cermak, J.E. and Cochran, L. (1992), "Physical modeling of atmospheric surface layer", *J. Wind Eng. Ind. Aerodyn.*, **41-44**, 935-946.
- Tieleman, H.W., Surry, D. and Mehta, K.C. (1996), "Full/model scale comparison of surface pressures on the Texas Tech experimental building", *J. Wind Eng. Ind. Aerodyn.*, **61**, 1-23.
- Levitan, M.L. and Mehta, K.C. (1992), "Texas Tech field experiments for wind loads part 1: building and pressure measuring system", *J. Wind Eng. Ind. Aerodyn.*, **41-44**, 1565-1576.
- Bienkiewicz, B. (1992), "Local wind loading on the roof of a low-rise building", *J. Wind Eng. Ind. Aerodyn.*, **45**, 11-24.
- Banks, D., Meroney, R.N., Sarkar, P.P., Zhao, Z. and Wu, F. (2000), "Flow visualization of conical vortices on flat roofs with simultaneous surface pressure measurement", *J. Wind Eng. Ind. Aerodyn.*, **84**, 65-85.
- Arie, M. and Rouse, H. (1956), "Experiments on two-dimensional flow over a normal wall", *J. Fluid Mech.*, **1**(Pt. 2), 129-141.
- Wilson, D.J. (1979), "Flow patterns over flat-roofed buildings and application to exhaust stack design", *ASHRAE Trans.*, **85**(Pt. 2), 284-295.